Journal of Materials and Electronic Devices 2 (2022) 12-19

JOURNAL OF MATERIALS AND ELECTRONIC DEVICES
FYTRONIX JMED
http://dergi-fytronix.com/

Cluster adsorption ability of small zigzag C_3N nanoribbons: A DFT Study

Serap Senturk Dalgic

[1]Trakya University, Department of Physics, Edirne, Turkey

In this work, the Cu_4Pd_2 cluster adsorption on the small zigzag C_3N nanoribbons (Z-C_3NNR) has been investigated by the density functional theory (DFT) method. The atomic structure of the Z-C_3NNR is formed from the honeycomb structure of the 2D-C_3N monolayer, with carbon atoms in the centre and n=4 zigzag edges (4Z-C_3NNR). The frontier molecular orbitals (FMO), the charge and density of states (DOS), the charge density difference (CDD) and Electron Localization Function (ELF) of pristine 4Z-C_3NNR, Cu_4Pd_2 cluster and Cu_4Pd_2/4Z-C_3NNR complex have been obtained with DFT/QE calculations.

The results indicate that the Cu_4Pd_2 cluster adsorption on the presented atomic configuration of 4Z-C_3NNR is an exothermic character. The complex structure of Cu_4Pd_2/4Z-C_3NNR exhibits semi-conductivity with the bandgap of 0.405 eV. Based on the changes in the work function of the complex, the 4Z-C_3NNR is sensitive to the cluster and a candidate for the work function type sensor for Cu-Pd clusters. There is a weak physical interaction between the adsorbed Cu_4Pd_2 and the 4Z-C_3NNR surface. However, the complex obtained by the interaction of Cu_4Pd_2 with 4Z-C_3NNR can more easily accept an electron from a system than the Cu_4Pd_2 cluster surface alone. Thus, the presented Cu_4Pd_2/ 4Z-C_3NNR structure can be applied to improve molecular hydrogen adsorption and hydrogen storage.

Keywords: *zigzag* C_3N *nanoribbons, Cu_n-Pd_m clusters, DFT, Quantum Espresso*

Submission Date: 23 March 2022
Acceptance Date: 10 May 2022

**Corresponding author: serapd@trakya.edu.tr , dserap@yahoo.com*

1. Introduction

The two-dimensional (2D) nanomaterials have great attention because of their unique properties, which differ from their bulk structure in 3D [1,2]. Recently, the new 2D nanomaterials composed of group IV and V elements greatly interest material science [3]. Among them recently synthesized [4], 2D polyaniline with a stoichiometric formula of C_3N is the most popular because of its tuneable structural, electronic and magnetic properties [5-13]. Although C_3N monolayer was first reported as a semiconductor, it was shown that its properties could be modulated by adatoms [9], functionalization [10], and hydrogenation [11], as a promising candidate nanosensor. The adsorption behaviours of different molecules on the C_3N nanosheets have investigated [10, 14-16].

These studies have shown that, compared to pure graphene, it has been suggested that C_3N may have a high chemical activity towards certain adsorbed gas molecules.

On this line, 2D-C_3N Nano sheet (NS) and 1D (one dimensional) nanoribbon (NR) and nanotube (NT) shaped C_3N nanostructures have particular attention to the possibility of indirect gap transition [17-24].

Among the C_3N nanostructures, the C_3N nanoribbons (C_3NNR) are of particular interest. Due to their unique edge effect, quantum confinement and magnetic ordering, they can offer more excellent electronic tunability than other C_3N nanostructures [19-23]. Because of their magnetic properties, (C_3NNR) are candidate for spintronic devices [19]. By converting 2D Nanosheets to 1D nanoribbons, the

fundamental changes occur in material properties due to the dimensional effect.

When the size of the material is reduced to quantum size, the quantum confinement effect occurs with the finite width of the ribbon.

Therefore, nanoribbons' electrical, electronic and adsorption properties are affected by the cutting direction, nanoribbon width and the functionalizing of the edge states [17,18, 20]. The morphological effect in nanoribbons and different edge states or configurations cause nanomaterial properties changes. Thus, 1D nanoribbons are crucial in developing new generation materials and their applications in nanotechnology.

According to edge structure, C_3NNR are classified as zigzag and armchair type nanoribbons representing Z-C_3NNR and A-C_3NNR, respectively. The edge state effect on the material properties of C_3NNR, such as atomic, electronic and magnetic, has been studied by some researchers [17-23]. Analogous to the graphene nanoribbons, C_3NNR can be formed by cutting the 2D C_3N nanosheet along the armchair, and zigzag directions of the binary C_3N system; there are three kinds of edges, that is, the pure C edges (CC), pure N edges (NN) and the CN edges with alternated C and N atoms.

Tagani et al. [17] investigated the electronic and magnetic properties of n- C_3NNR with n=8-18, where n denotes C_3NNR having n C-N pairs in their unit cell. Ding et al. [18] have reported the possible 22 types of edge structures in C_3NNR. Li et al. [19] first reported the host spin-polarized electronic edge states of H-passivated zigzag C_3NNR that edges composed of both C and N atoms (ZZ-CN/CN) are semiconductors, and their bandgaps decrease with the enlargement of ribbon width. Bafekry et al. [20] studied the variation in the atomic, structural, electronic and magnetic properties of n- C_3NNR with n=4-11, depending on the nanoribbon edge states and width and demonstrated that the bandgaps of Z- C_3NNR and A- C_3NNR s converge to different values with the increase of width.

Furthermore, some researchers [21-23] studied the edge morphology-induced rectifier diode effect in Z-C_3NNR. It has been reported that if both edges are not of all-carbon morphology due to N atoms, a forward-conducting and reverse blocking rectifier diode behaviour will appear. Xia et al. [22] reported that the H-passivated Z-C_3NNR with edges composed of both C and N atoms are semiconductors, and their bandgaps decrease tend to a constant, which is the value of nanosheet when the width is large enough.

When considering all these studies, Z-C_3NNR are a very important subject in material science. On the other hand, among Z-C_3NNR, there is such a structure, the smallest (narrowest) of which is 4Z-C_3NNR, that it has been reported to have extraordinary properties by some researchers [19,24]. Li et al. [19] studied the narrowest Z-C_3NNR of 4Z-C_3NNR with the configurations of the edge sites occupied with three C and one N atoms displaying very high spin polarization. That configuration is the CCCN edge one, also studied by Bafekry et al. [20]. The calculated band gaps for 4Z- C_3NNR with CCCN edge is about 1.20e V and 1.25 e V, respectively.

In our previous work [24], the narrowest 4Z-C_3NNR was presented with a different configuration than others, where carbon atoms were placed at the centre. It has been found in our previous work that the band gap of the presented configuration is close to the C_3N nanosheet.

In this work, the cluster adsorption ability of the narrowest 4Z-C_3NNR has been presented by spin-unpolarised DFT calculations. For this purpose, the Cu_4Pd_2 alloy cluster was considered. In a recent study, Herranz et al. [25] presented Cu-Pd alloys' molecular hydrogen adsorption ability. They concluded that it is relevant for hydrogen storage on porous carbon materials. On this line, based on the results in this work, the 4Z-C_3NNR improves the electron accepting capability of the Cu_4Pd_2 alloy cluster.

2. Materials and Method

In this work, the Z-C_3NNR was used as a nanosurface. It was created as follows: The honeycomb structure of 2D- C_3N monolayer with optimized lattice constant is 4.861Å, which agrees well with the previous calculations [6-8]. The bond lengths of carbon atoms C-C (d CC) and carbon-nitrogen atoms C-N (d NC) are 1.403Å and 1.4029Å in the optimized 2D- C_3N monolayer, respectively. The 4Z-C_3NNR produced from the optimized 2D-honeycomb C_3N monolayer is used in our calculations. Here, the Cu_4Pd_2 cluster with zero spin magnetic moment is selected as an adsorbed molecule and is shown in Fig. 1.

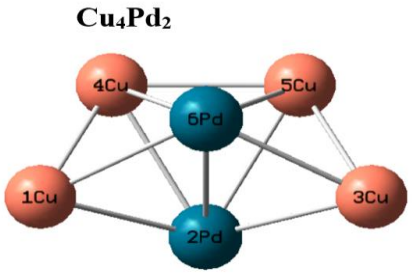

Fig.1. The top view of optimized atomic structure of Cu_4Pd_2 cluster. Orange and dark green spheres represent Cu and Pd atoms, respectively

The shape given in Fig. 1 is chosen for the Cu_4Pd_2 cluster, which is obtained as the ground state structure with the lowest energy in previous calculations [25]. Furthermore, the molecular hydrogen capture ability of the Cu_4Pd_2 cluster was also reported [25]. We have performed density

functional theory (DFT) with Quantum Espresso code [26]. The Perdew-Burke-Ernzerhof generalized gradient approximation (GGA-PBE) has been used for the exchange-correlation, and to deal with electron-ion core interactions, the projected augmented wave method (PAW) has been employed. Cut-off energy of 45 Ry was selected for the plane waves used to expand the Kohn-Sham orbitals and 350 Ry for the charge density. The automatic k point is used. Van der Waals corrections have been considered using the Grimme-D3 method [26].

The adsorption energy of the Cu_4Pd_2 cluster on 4Z-C_3NNR was computed as follows [27]:

$$E_{ads} = E(complex) - E(cluster) - E(nanoribbon). \quad (1)$$

where E(complex), E(cluster) and E(nanoribbon), are the total energies of complex, Cu_4Pd_2 cluster and 4Z-C_3NNR, respectively.

The recovery time (τ) (or desorption time) for the adsorbed cluster on the 4Z-C_3NNR surfaces can be described by

$$\tau = \upsilon^{-1}\exp\left(-\frac{E_{ads}}{kT}\right) \quad (2)$$

where υ is the attempt frequency, k_b is the Boltzmann constant and T is temperature [28].

The Chemical stability of the material was mainly influenced by the highest occupied molecular orbital (HOMO) and the lowest unoccupied molecular orbital (LUMO), where the HOMO and LUMO levels play an essential role in its electrical properties. Band gap energy, Eg can be expressed in terms of E_{LUMO} and E_{HOMO} energies as follows:

$$E_g = E_{LUMO} - E_{HOMO} \quad (3)$$

and $\%\Delta E_g$ is the percentage variation in the energy gap of E_g complex (Cu_4Pd_2 /4Z-C_3NNR) after adsorption with respect to the bare nanoribbon (4Z-C_3NNR) given by;

$$\%\Delta E_g = [(E_g(complex) - E_g(4Z\text{-}C_3NNR))/E_g(4Z\text{-}C_3NNR)] * 100. \quad (4)$$

The electrical conductivity of a material can be determined as:

$$\sigma \propto \exp\left(-\frac{E_g}{2k_bT}\right) \quad (5)$$

where E_g is the bandgap, T is the temperature, k_b is the Boltzmann constant. The sensitivity of material as:

$$\%S = \frac{|\sigma_{nanoribbon} - \sigma_{complex}|}{\sigma_{nanoribbon}} \times 100 \quad (6)$$

where $\sigma_{nanoribbon}$ is the conductivity of nanoribbon, $\sigma_{complex}$ is the conductivity of the complex structure. The Fermi energy level (E_F) is calculated by;

$$E_F = E_{HOMO} + (E_g/2). \quad (7)$$

The work function (Φ) is a significant factor for sensor materials. It is defined as the minimum amount of energy needed to remove an electron from the Fermi level of a material to an infinite distance and is given as follows,

$$\Phi = -E_F. \quad (8)$$

Parameters related to E_{LUMO} and E_{HOMO} energies such as chemical potential (μ), hardness (η), electronegativity ($\varkappa$), electrophilicity index (ω), nucleofugality (ΔE_n), electrofugality (ΔE_e), maximum electron flow (ΔN_{max}) were calculated using the following equations.

$$\mu = -\chi \cong \left(\frac{E_{HOMO}+E_{LUMO}}{2}\right) \quad (9)$$

$$\eta = \frac{E_{LUMO}-E_{HOMO}}{2} \quad (10)$$

$$\omega = \frac{\mu^2}{2\eta} \quad (11)$$

$$\Delta E_n = \frac{(\mu+\eta)^2}{2\eta},\ \Delta E_e = \frac{(\mu-\eta)^2}{2\eta},\Delta N_{max} = -\frac{\mu}{\eta} \quad (12)$$

In order to understand the electronic properties of pristine 4Z-C_3NNR and Cu_4Pd_2/4Z-C_3NNR complex, the DOS, Charge density difference (CDD) and electron localized function (ELF) have been obtained by the self-consistent field (SCF)-DFT/ QE calculations. Charge transfer analysis between nanoribbon and Cu_4Pd_2 cluster was calculated through the total charge density difference $\nabla\rho(\boldsymbol{r})$, in accordance to;

$$\rho_{diff}(\boldsymbol{r}) = \rho_{comp.}(\boldsymbol{r}) - \rho_{cluster}(\boldsymbol{r}) - \rho_{nanoribbon}(\boldsymbol{r}) \quad (13)$$

where $\rho_{complex}(\boldsymbol{r})$ is the charge density for complex structure, while $\rho_{cluster}(\boldsymbol{r})$, $\rho_{nanoribbon}(\boldsymbol{r})$ are the charge densities of the isolated Cu_4Pd_2 cluster, and pristine nanoribbon, respectively [29]. The isosurface of charge density difference was depicted by using the VESTA program [30].

The electron localization function (ELF) is a valuable tool to determine the location of electron pairs to understand the nature of the chemical bonding and discuss the mechanism of chemical reactions [31,32]. The ELF analysis for the Cu_4Pd_2 cluster on the 4Z-C_3NNR surface has been presented.

3. Results and Discussions

Optimised Structures and Adsorption Properties

As indicated in the previous section, the C_3N nanoribbon studied in this work was formed from hexagonal hydrogen-terminated C_3N nanosheet (C3NNS) by cutting along the x directions. For this reason, the atomic structure of 4Z-C_3NNR has a different atomic profile of carbon and nitrogen atoms compared with others [19,20]. The charge analysis for nanoribbons is an important issue in understanding their electronic and optical properties. After the relax calculations, the charged values of the optimized cluster and complex structure are presented in Fig. 2a-b. Löwdin charges were calculated by the Löwdin atom and basis function population using QE code. Note that Fig. 2 shows partial charges in the system despite natural ones.

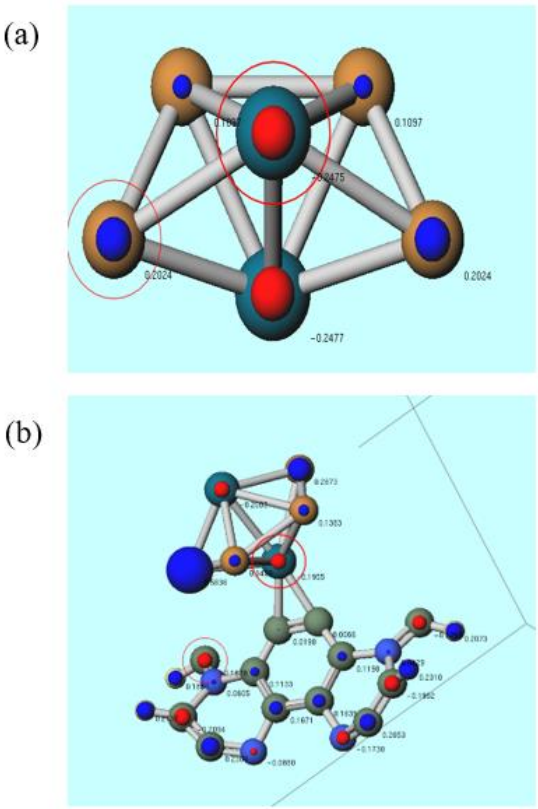

Fig.2. The Löwdin charges of optimized (a) Cu_4Pd_2 cluster and (b) Cu_4Pd_2 /4Z-C_3NNR complex structure.

The optimized structure of the bare cluster, as shown in Fig. 2a, is a pentagonal bipyramid geometry consistent with the literature [25]. As shown in Fig. 2a, Pd atoms get an electronic charge from Cu atoms in the Cu_4Pd_2 cluster; as a result, they have a negative electronic charge indicated before. In Fig. 2b, the Pd atom in Cu_4Pd_2 is temporarily bonded to carbon atoms in the nanoribbon's centre.

The charge values of carbon atoms in the complex structure are 0.0196e (left) and 0.0066 (right), whereas those values are 0.0685e for carbon atoms placed at centred(left) and (right) of pristine nanoribbon as given in our previous study [24]. It is clear that small charge transfers between the cluster Cu_4Pd_2 and nanoribbon surface.

On the other hand, the adsorption energy E_{ads} of the Cu_4Pd_2 cluster E_{ads} (Cu_4Pd_2) on the presented 4Z-C_3NNR configuration has been calculated using Equation (l) as -2.902 eV. Adsorption energy was calculated as the difference between the total energy of the complexes formed between nanoribbon and cluster, and the sum of the total energies of the isolated nanoribbon and isolated cluster.

The adsorption of the Cu_4Pd_2 cluster on 4Z-C_3NNR is an exothermic process that means physisorption type adsorption has occurred. Fig.1 shows the short-term interaction moment of the cluster and nanoribbon. The closest distance between cluster and nanoribbon is about 2.0Á. The recovery time (τ) value in sec was obtained by Eq.(2) at room temperature (298K) using the UV vacuum light with the frequency of $\upsilon \sim 3x10^{12}$ s^{-1} . The calculated τ(sec)= 3.98 x 10^{36}. Depending on the adsorption energy, the highest recovery or desorption time indicates nanoribbon's ability to store Cu-Pd clusters.

Frontier Molecular Orbitals (FMO), Electrical and Electronic Properties

The obtained HOMO and LUMO orbitals of complex is illustrated in Fig. 3

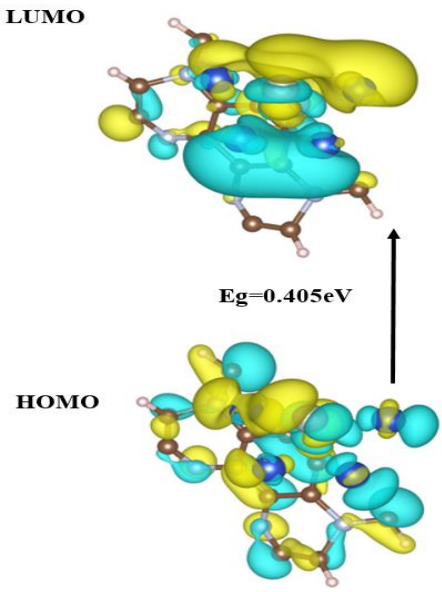

Fig.3. The HOMO and LUMO schematic graphs for the Cu_4Pd_2 /4Z-C_3NNR complex structure.

It is evident in Fig. 3 that all atoms in complex structure contributed to HOMO, whereas the main contributor to LUMO is from the Cu_4Pd_2 cluster. This supports the presented results in the following sections.

The electronic and physicochemical properties of Cu_4Pd_2 /4Z-C_3NNR complex by comparison with the Cu_4Pd_2 and 4Z-C_3NNR results are tabulated in Table1 and Table2, respectively.

Table 1. E_{LUMO} and E_{HOMO} energies, Band gap energy, E_g and work function Φ, percentage variation in band gap energy (%ΔE_g) and work function (%ΔΦ), sensitivity %S values (All energies are in eV).

Properties	Cu_4Pd_2	4Z-C_3NNR	Cu_4Pd_2 / 4Z-C_3NNR
E_{HOMO}	-3.846	-4.722	-4.317
E_{LUMO}	-3.411	-4.333	-3.912
E_g	0.435	0.389	0.405
$\%\Delta E_g$	-	-	4.113
$\Phi = -E_F$	3.629	4.528	4.115
%ΔΦ	-	-	-9.121
%S	-	-	79.503

Although the E_{LUMO} values of cluster and complex are less negative than those obtained from the E_{LUMO} value of 4Z-C_3NNR, as it is known during molecular interactions, the LUMO, corresponding to the electron affinity, accepts electrons. The Eg energy gap is important in determining the charge transfer interaction and molecular electrical transport properties within the molecule. A molecule with a high energy gap means low chemical reactivity and high kinetic stability. As observed in Table 1, the pristine 4Z-C_3NNR with the lowest Eg value exhibits more chemical reactivity than the cluster. The % ΔEg of the complex is about %4.113 with respect to the bare nanoribbon. Thus, the energy band gap of complexes increases after adsorption. However, there is a decrease in the work function of about %9.121. The lower Eg values indicate higher electrical conductivity, reactivity and sensitivity that can be obtained in Eq. 5. It is evident in Table 1 that the 4Z-C_3NNR is sensitive (%S) to the Cu_4Pd_2 cluster.

The complex structure of Cu_4Pd_2 / 4Z-C_3NNR has a higher Eg energy gap than pristine 4Z-C_3NNR. It is stable and chemically harder than pristine nanoribbon having a small Eg energy gap. As seen in Table 2, the Cu_4Pd_2 cluster is the hardest one (0.218) and the most stable (less reactive), while 4Z-C_3NNR is the softest (0.194) and the least stable of all in the studied nanostructures. The global hardness (η) of the Cu_4Pd_2 / 4Z-C_3NNR complex system increased.

Table 2. Physicochemical properties of bare Cu_4Pd_2 cluster, pristine 4Z-C_3NNR and Cu_4Pd_2/4Z-C_3NNR complex.

Properties	Cu_4Pd_2	4Z-C_3NNR	Cu_4Pd_2 / 4Z-C_3NNR
μ	-3.629	-4.528	-4.115
η	0.218	0.194	0.202
ω	30.256	52.754	41.816
ΔE_e	33.993	57.378	46.032
ΔE_n	26.736	48.323	37.802
ΔN_{max}	16.676	23.303	20.325

With the electronic chemical potential of the nanostructures, the direction of charge transfer is completely determined

The electrophile index (ω) exhibits the chemical type of the system that can accept electrons from the environment. The high electrophile index (ω) of 52.754 demonstrates that the electron-accepting capability of the studied 4Z-C_3NNR is superior. On the other hand, the complex structure's electrophile index (ω) increases after adsorption with a value of 41.816. It is consistent with other values given in Table 2. A molecule with a high nucleofugality (ΔEn) readily accepts an electron from a system; conversely, if a molecule has a high electrofugality (ΔEe), it readily donates an electron to the system. The ΔEn value of the complex is increased % by 38.69 with respect to the cluster surface means that the complex obtained between the interaction of Cu_4Pd_2 with 4Z-C_3NNR can accept an electron more easily from a system than alone Cu_4Pd_2 cluster surface. In comparison, the percentage increase in ΔEe with respect to the cluster is about %35.41. ΔN_{max} determines the ability of the system to obtain additional electronic charges from the medium that defines the charge capacity of the system. The obtained value of ΔN_{max} for the complex is about 20.325, which is higher than that of the bare cluster. It is consistent with the other results above.

In order to understand the electronic nature of the system, we have calculated the density of states (DOS) of the Cu_4Pd_2 / 4Z-C_3NNR complex structure. The DOS of the bare cluster and the pristine 4Z-C_3NNR have been compared. The total DOS for the bare cluster and studied complex structure is given in Fig. 4, along with those obtained for the pristine 4Z-C_3NNR.

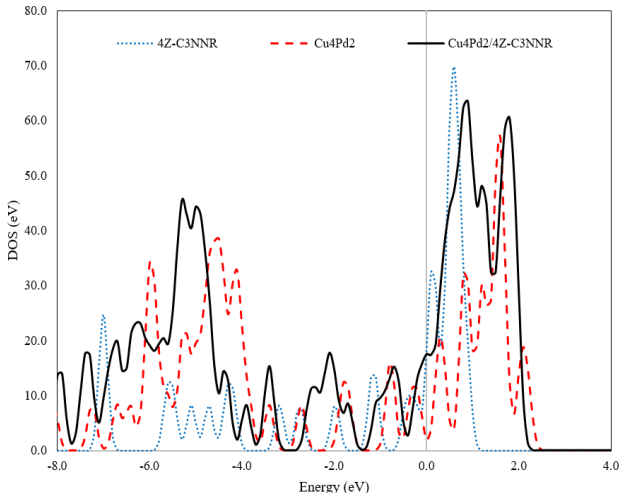

Fig.4. The calculated total DOS graphs of bare cluster, 4Z-C_3NNR and complex structure.

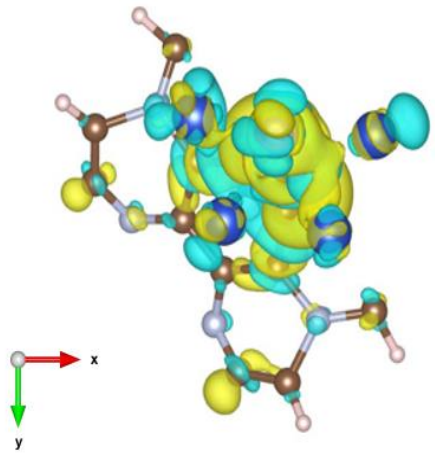

Fig.5. Top view for the CDD function of the Cu_4Pd_2/4Z-C_3NNR complex structure. The isosurface value is 0.01 e/$A^{\circ 3}$.

In Fig. 4, it was observed that there was a slight overlap between the electron density of the adsorbed Cu_4Pd_2 and that of the 4Z-C_3NNR indicating that the Cu_4Pd_2 interacted with the 4Z-C_3NNR surface in -3.0 and -2.4 e V energy range. It was reasonable to infer that there was only a weak physical interaction between the adsorbed Cu_4Pd_2 and the 4Z-C_3NNR surface for the bridge position.

On the other hand, there is no high peak of DOS across the EF level for the presented configuration of 4Z-C_3NNR with spin-unpolarised calculations. Thus, the 4Z-C_3NNR system is stable based on the Stoner criterion, which implies the EF for the non-magnetic system exhibits a very high unstable peak [19]. The same steady state is observed in the DOS graph of the Cu_4Pd_2 cluster, which was found to have no magnetic moment in previous spin-polarized calculations [25]. Our results are compatible with the literature in this respect.

Charge Density Difference (CDD) and Electron Localization Function (ELF)

To gain further insight into the adsorption of the Cu_4Pd_2 cluster on the 4Z-C_3NNR, we have calculated the charge density difference (CDD) profiles. Fig. 5 also shows the CDD of the Cu_4Pd_2 cluster onto the nanoribbon. Blue regions represent charge depletion, while yellow regions represent charge accumulation. The CDD plot depicts the charge redistribution between the bonding regions of the nanoribbon and Cu_4Pd_2 cluster. In Fig.5, blue spheres show the Cu atoms; brown, grey, dark grey and pink spheres are carbon, nitrogen, palladium and hydrogen atoms, respectively.

In Fig. 5, the yellow region indicates electron accumulation, and the blue region shows electron depletion. The electropositive charge density (or charge depletion) is observed around Cu atoms located on the carbon atoms centred on the surface. A small electron depletion charge was observed around the nanoribbon's surface carbon and nitrogen atoms.

In Fig. 5, the electronegative charge density is observed on the complex's top and bottom of the Cu_4Pd_2 cluster, indicating Pd atoms (at the top and bottom position). The Löwdin charge graphs in Fig. 2 support CDD results.

The CDD revealed an increase in charge accumulation and depletion in some regions of the 4Z-C_3NNR surface compared to the pure 4Z-C_3NNR surface to more effectively interact with the cluster.

Furthermore, the electron localization function (ELF) also is shown in Figure 6. ELF is a popular function to reveal electron localization character in determining the localization of electron pairs probability. It gives information to understand the behaviours of electrons in multielectronic systems.

ELF provides information about binding and the location of bonds. The probability density of finding another electron with the same spin near the reference electron is related to the electron density. This approach allows for deciding the localization of electrons. The ELF values can be obtained in a more desirable range of [0-1]. The ELF value varies in the range [0,0.5] for the delocalized electrons, whereas an ELF value of >0.5 for perfect localized ones.

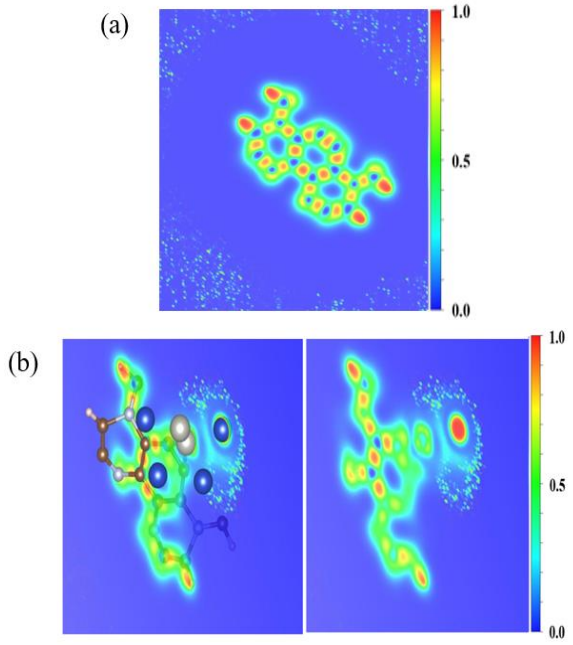

Fig.6. ELF function for (a) the 4Z-C_3NNR and (b) Cu_4Pd_2/4Z-C_3NNR complex structure. The isosurface value is 0.01 e/A°^{3}.

The ELF scale is shown on the right-hand side in Fig.6. In Fig. 6b, it was observed from ELFs of Cu_4Pd_2/4Z-C_3NNR complex structure that two dark blue areas seen in the ELF of the 4Z-C_3NNR in Fig. 6a remain in the lower plane. It indicates the interaction between the Cu_4Pd_2 cluster and 4Z-C_3NNR surface that electron localization decreases in those regions. The larger area of the dark blue region on the 4Z-C_3NNR of Cu_4Pd_2/ 4Z-C_3NNR complex structure than that of pristine 4Z-C_3NNR indicates charge transfer by weak interaction during the adsorption of a Cu_4Pd_2 cluster on the 4Z-C_3NNR surface.

4. Conclusion

DFT calculations discussed the adsorption energy, geometric structure, and electronic and physicochemical properties of the Cu_4Pd_2 cluster on the 4Z-C_3NNR. The charge density and DOS were also calculated and analyzed to understand the electronic properties of the system. The charge distribution and the nature of interactions were discussed using the charge density difference and electron localization functions.

The calculated considerable negative adsorption energy is in a comparable range to the previous calculations. A weak interaction between the 4Z-C_3NNR surface and the Cu_4Pd_2 cluster was observed. The long desorption time for the Cu_4Pd_2 cluster at room temperature has been found that the proposed atomic structure shows superior storage capability of Cu-Pd clusters.

When the Cu_4Pd_2 cluster is adsorbed on the 4Z-C_3NNR, its work function decreases significantly, showing a good sensitivity. Thus, the 4Z-C_3NNR surface has potential applications as a work function-type sensor for the Cu-Pd alloy clusters.

Furthermore, the electron accepting ability of the Cu_4Pd_2 cluster increases when the cluster forms a complex with the 4Z-C_3NNR. Finally, the Cu_4Pd_2/4Z-C_3NNR complex structure may use to improve hydrogen storage in future applications.

References

[1] H. Zhang, Ultrathin Two-Dimensional Nanomaterials ACS Nano 9 (2015) 9451-9469

[2] B. Liu, K. Zhou, Recent progress on graphene-analogous 2D nanomaterials: Prop., modelling and applications, Prog. in Materials Science, 100 (2019) 99-169.

[3] T. Wang, K. Lu, Z. Li, L. Dai, J. Yin, Strain-engineering on mechanical and electronic properties of group IV-V two dimensional semiconductors., Mater. Res. Express 8 (2021) 105006.

[4] J. Mahmood, E. K. Lee, M. Jung, D. Shin, H.-J. Choi, J.-M. Seo, S.-M. Jung, D. Kim, F. Li, M. S. Lah, N. Park, H.-J. Shin, J. H. Oh, J.-B. Baek, two dimensional Polyaniline (C_3N) carbonized organic single crystals in solid state, PNAS 113 (2016) 7414.

[5] S. Senturk Dalgic, 2D PANI/GOLD Nanocomposites: A Molecular Dynamics Study, Proc. of 4th International Organic Elec. Mater. Technology Conf. (OEMT 2019) 1-5.

[6] S. Mizuno, M. Fujita, K. Nakao, Electronic States of Graphitic Heterocompounds of Carbon, Boron and Nitrogen, Synth. Met. 71 (1995) 1869.

[7] H. Qianku, W. Qinghua, W. Haiyan, H. Julong, Z. Guanglei, First-Principles Studies of Structural and Electronic Properties of Layered C3N Phases. Phys. Status Solidi B, 249 (**2012)** 784.

[8] B. Mortazavi, Ultra High Stiffness and Thermal Conductivity of Graphene Like C_3N, Carbon 118 (2017) 25.

[9] M. Makaremi, B. Mortazavi, C. V. Singh, Adsorption of Metallic, Metalloidic, and Nonmetallic Adatoms on Two-Dimensional C_3N, J. Phys. Chem. C, 121 (**2017)** 18575.

[10] A. Bafekry, C. Stampfl, S. Farjami Shayesteh, F. M. Peeters, Expliting the novel Electronic and Magnetic Structure of C_3N via Functionalization and Conformation, Adv. Electron. Mater., 5 (2019) 1900459.

[11] M. B. Tagani, Electrical and Mechanical Properties of a Fully Hydrogenated Two Dimensional Polyaniline Sheet. Comput. Mater. Sci., 153 (**2018)** 126.

[12] S. Yang, W. Li, C. Ye, G. Wang, H. Tian, C. Zhu, P. He, G. Ding, X. Xie, Y. Liu, Y. Lifshitz, S.-T. Lee, Z. Kang, M. Jiang, C3N—A 2D Crystalline, Hole-Free, Tunable-

Narrow-Bandgap Semiconductor with Ferromagnetic Properties, *Adv. Mater.* 29 (**2017)** 1605625.
[13] X. Zhou, W. Feng, S. Guan, B. Fu, W. Su, Y. Yao, Computational characterization of monolayer C3N: A two-dimensional nitrogen-graphene crystal*J. Mater. Res.* 32 (**2017)** 2993.
[14] M. Pashangpour, A. A. Peyghan, Adsorption of Carbon Monoxide on the Pristine, Band Al-Doped C_3N Nanosheets. J. Mol. Model. 21 (**2015**) 116.
[15] Y. Lv, Y. Wang, H. Zhang, C. Dai, Adsorption of NH_3 and NO_2 molecules on the carbon doped C_3N monolayer: A first principles study, Comput. Theo. Chem., 1195 (2021) 113075.
[16] S. Senturk Dalgic, F. Kandemirli, DFT based calculations of Acid Molecules on 2D-C_3N Nanosheets: QTAIM, NCI analysis, J. Mater. Electron. Device. 5 (2021) 1.
[17] M. Bagheri Tagani, S. I. Vishkayi, Polyaniline (C_3N) nanoribbons: Magnetic metal, semiconductor, and half-metal J. Appl. Phys. 124 (2018) 084304.
[18] Y. Ding, Y. Wang, Stable H-Terminated Edges, Variable Semiconducting Properties and Solar Cell Applications of C_3N nanoribbons: A first-principles Study, ACS Omega 3 (2018) 8777.
[19] Q. Li, H. Wang, H. Pan, Y. Ding, Tunable electronic structures and magnetic properties of zigzag C3N nanoribbon, J. Phys. D: Appl. Phys. 51 (2018) 345301
[20] A. Bafekry, C. Stampfl, S. Farjami Shayesteh, A First Principles Study of C_3N Nanostructures: Control and Engineering of the Electronic and Magnetic Properties of Nanosheets, Tubes and Ribbons, ChemPhysChem, 27 (2020) 164.
[21] J-J He, Y-D Guo, X-H Yan, H-Li Zheng, Edge morphology induced rectifier diode effect in C3N nanoribbon, Phys. Chem. Chem. Phys., 20 (2018) 28759.
[22] C. X. Xia, L. Z. Fang, W. Q. Xiong, T. X. Wang, S. Y. Wei, Y. Jia, Rectification effects of C_3N nanoribbons-based Schottky junctions, Carbon. 141 (2019) 363
[23] Y. Ren, F. Cheng, X. Y. Zhou, K. Chang, G. H. Zhou, Tunable mechanical, electronic and magnetic properties of monolayer C_3N nanoribbons by external fields, Carbon 143 (2019) 14
[24] S. Senturk Dalgic, DFT calculations on the small zigzag C3N nanoribbons, J. Mater. Electron. Device. 6 (2021) 16.
[25] A. Gomez Herranz, E. German, J. A. Alonso, M. J. Lopez, Interaction of hydrogen with palladium-copper nanoalloys, Theoretical Chem. Accounts, 140 (2021) 35.
[26] P. Giannozzi, O. Andreussi, T. Brumme, O. Bunau, M. Buongiorno Nardelli, M. Calandra, R. Car, C. Cavazzoni, D. Ceresoli, M. Cococcioni, N. Colonna, I. Carnimeo, A. Dal Corso, S. de Gironcoli, P. Delugas, R. A. DiStasio Jr, A. Ferretti, A. Floris, G. Fratesi, G. Fugallo, R. Gebauer, U. Gerstmann, F. Giustino, T. Gorni, J Jia, M. Kawamura, H.-Y. Ko, A. Kokalj, E. Küçükbenli, M .Lazzeri, M. Marsili, N. Marzari, F. Mauri, N. L. Nguyen, H.-V. Nguyen, A. Otero-de-la-Roza, L. Paulatto, S. Poncé, D. Rocca, R. Sabatini, B. Santra, M. Schlipf, A. P. Seitsonen, A. Smogunov, I. Timrov, T. Thonhauser, P. Umari, N. Vast, X. Wu, S. Baroni, Advanced capabilities for materials modeling with Quantum ESPRESSO, Journal of Physics: Condensed matter, 29(46) (2017) 465901. https://doi.org/10.1088/1361-648X/aa8f79
[27] H. S. Sayiner, F. Kandemirli, S. Senturk Dalgic, M. Monajjemi, F. Mollaamin, Carbazochrome carbon nanotube as drug delivery nanocarrier for anti-bleeding drug: quantum chemical study, J. Mol. Modelling 28 (2022) 11-26.
[28] Zaid H. Al-Sawaff, Serap Senturk Dalgic, Zaheda A. Najim, Shatha S. Othman, Fatma Kandemirli, A comparative Density Functional Theory Study of BMSF-BENZ Chemisorption on $Zn_{12}O_{12}$ and $Al_{12}P_{12}$ nanocages, Phys. Chem. Solid State, 23(1) (2022) 120-133.
[29] C. A. Celaya, M. Boujnah, M. Reina, J. Muniz, L. E. Sansores, Theoretical study of Au_{20}/WS_2 composite material as a potential candidate for the capture of XO (X=C, N, S) gases, Computational Condensed Matter, 25 (2021) e00580.
[30] K. Momma and F. Izumi, *VESTA 3* for three-dimensional visualization of crystal, volumetric and morphology data, J. Appl. Crystallogr., 44 (2011) 1272-1276. https://doi.org/10.1107/S0021889811038970
[31] A. D. Becke and K. E. Edgecombe, A simple measure of electron localization in atomic and molecular systems, J. Chem. Phys., 92 (1990) 5397.
[32] E. Matito, Electron localization function at the correlated level, The Journal of Chemical Physics, 125 (2006) 024301.